International Journal of Remote Sensing
Vol. 26, No. 3, 10 February 2005, 457–474

Taylor & Francis
Taylor & Francis Group

EO-1 Hyperion, ALI and Landsat 7 ETM+ data comparison for estimating forest crown closure and leaf area index

R. PU*, Q. YU, P. GONG and G. S. BIGING
Center for Assessment and Monitoring of Forest and Environmental Resources (CAMFER), 151 Hilgard Hall, University of California, Berkeley, CA 94720-3110, USA

(*Received 1 September 2003; in final form 21 June 2004*)

In this study, mixed coniferous forest crown closure (CC) and leaf area index (LAI) were measured at the Blodgett Forest Research Station, University of California at Berkeley, USA. Data from EO-1 Hyperspectral Imager (Hyperion) and Advanced Land Imager (ALI) acquired on 9 October 2001, and from Landsat 7 Enhanced Thematic Mapper Plus (ETM+) on 25 October 2001 were used for estimation of CC and LAI. A total of 38 forest CC and LAI measurements were used in this correlation analysis. The analysis procedure consists of (1) atmospheric correction to retrieve surface reflectance from Hyperion, ALI and ETM+ data, (2) a total of 38 patches, corresponding to ground CC and LAI measurement plots, extracted from data from the three sensors, and (3) calculating univariate/multivariate correlation coefficient (R^2) and root mean square error (RMSE) using CC and LAI measurements and retrieved surface reflectance data of the three sensors. The experimental results indicate: (1) higher individual band correlations with CC and LAI appear in visible and short wave infrared (SWIR) regions due to spectral absorption features (pigments in visible and water and other biochemicals in SWIR); (2) based on ALI individual band wavelengths, the R^2/RMSE produced with Hyperion bands are all better than those with ALI, except ALI band 1, due to atmospheric scattering of Hyperion bands in the visible region; (3) based on ETM+ individual band wavelengths, Hyperion is better than ALI, which is better than ETM+, especially for the NIR band group of Hyperion; (4) based on spectral region, Hyperion, again, is better than ALI which is better than ETM+, and optimal results appear in the visible region for ALI and in SWIR for Hyperion; and (5) if considering just six bands or six features (six principal components) in estimating CC and LAI, optimal results are obtained with six bands selected from the 167 Hyperion bands. In general, for estimation of forest CC and LAI in this study, the Hyperion sensor has outperformed the ALI and ETM+ sensors, whereas ALI is better than ETM+. The best spectral region for Hyperion is SWIR, but for ALI and ETM+, the visible region should be considered instead.

1. Introduction

The primary mission of Earth Observing-1 (EO-1) is to develop and validate instruments and technologies for space-based Earth observation with unique spatial, spectral and temporal characteristics not previously available. Three revolutionary

*Corresponding author. Email: rpu@nature.berkeley.edu

International Journal of Remote Sensing
ISSN 0143-1161 print/ISSN 1366-5901 online
http://www.tandf.co.uk/journals
DOI: 10.1080/01431160512331299324

land imaging instruments: Advanced Land Imager (ALI), Atmospheric Corrector (AC) and Hyperspectral Imager (Hyperion), flown on the EO-1 satellite (Ungar *et al.* 2003) will collect multispectral and hyperspectral scenes over the course of its mission in coordination with the Enhanced Thematic Mapper Plus (ETM+) on Landsat 7. A significant part of the EO-1 programme is performing data comparisons among Hyperion, ALI and ETM+. The comparisons are ensured, since the EO-1 orbit matches the Landsat 7 orbit with only a 1-min delay. Typical comparisons might be concerned with absolute radiometric/reflectance (from the top of the atmosphere or from Earth's surface) (e.g. Barry *et al.* 2002, Bryant *et al.* 2002), or with applicability of various sensors' data (e.g. Goodenough *et al.* 2002). Barry *et al.* (2002) performed absolute radiometric comparisons among Hyperion, ALI and ETM+. The results demonstrated the capability of Hyperion to synthesize ALI and ETM+. After comparing the retrieved surface reflectances from ALI with those from Landsat ETM+ and Landsats 4 and 5 Thematic Mapper (TM) and considering the fact that ALI is a sensor launched for validation of new sensor technologies, Bryant *et al.* (2002) concluded that the ALI sensor performed extremely well. In monitoring forests with Hyperion, ALI and ETM+ images, Goodenough *et al.* (2002) compared capabilities of the data from the three sensors used for forest classification at various classification levels. Their experimental results indicated that Hyperion outperformed ALI and ETM+ in forest classification and that ALI classification results were much better than ETM+. In this analysis, we propose to compare the capabilities of the three sensors (Hyperion, ALI and ETM+) for estimating forest crown closure (CC) and leaf area index (LAI). This work contributes to validating EO-1 data for extracting biophysical parameters, such as CC, LAI and tree species.

We selected the two biophysical parameters (CC and LAI) as indicators for evaluating capabilities of the three sensors because both are important structural parameters for quantifying the energy and mass exchange characteristics of terrestrial ecosystems such as photosynthesis, respiration, transpiration, carbon and nutrient cycle, and rainfall interception (Gong *et al.* 1995, Chen and Cihlar 1996, Fassnacht *et al.* 1997, Gobron *et al.* 1997, White *et al.* 1997, Chen *et al.* 1999, Hu *et al.* 2000). LAI quantifies the amount of live green leaf material present in the canopy per unit ground area. It is defined as the total one-sided area of all leaves in the canopy within a defined region ($m^2\ m^{-2}$). CC can be defined as percentage of land area covered by the vertical projection of tree crowns. Reflectance spectra of a forest stand are the combined reflectance spectra of trees, ground vegetation and underlying soil. Forest reflectance directly depends on the proportions of these components (e.g. crown, grasses and bare soil) in a pixel or in the elementary surface viewed by a sensor (Guyot *et al.* 1989). Although CC is not studied as extensively as LAI in ecosystem science, since it is easily measured in the field and is viewed vertically by a sensor, estimation and mapping of CC with various remote sensing data are often conducted in forest inventory and ecosystem studies. For example, CC, estimated and mapped from aerial photographs, is an important element in timber management plan inventory (US Department of Agriculture 1968) and in forest resources inventory (Fang 1980). In addition, Gerylo *et al.* (2002) and Hall *et al.* (1998) successfully estimated forest CC using Landsat 5 TM image and airborne multispectral video camera images, respectively. Although CC has a different ecological significance than LAI, the two are closely correlated. Therefore, the CC is also used as a bio-parameter extracted from remote sensing. In this study,

mixed coniferous forest CC and LAI were collected at the Blodgett Forest Research Station, University of California at Berkeley, USA. Data from Hyperion, ALI and ETM+ were used to estimate the forest CC and LAI. The objectives of this study are to (1) compare capabilities of Hyperion, ALI and ETM+ for estimating forest CC and LAI and (2) find an optimal spectral region and band groups to be effective for estimating forest CC and LAI. This article is organized as follows: section 2 briefly describes the characteristics of the three sensors, section 3 describes the study site and data acquisition and measurement, and section 4 briefly describes comparison methods for evaluating the capabilities of the three sensors, including the sensors' data pre-processing. In section 5, we present, analyse and discuss the comparison results of the three sensors. Finally, in the last section, we summarize with several conclusions derived from this experiment.

2. The characteristics of three sensors

In this section, we will briefly describe the characteristics of the three sensors: Hyperion, ALI and ETM+. For a detailed description of EO-1 sensors (Hyperion, ALI and LAC) and the EO-1 mission, see Ungar *et al.* (2003).

2.1 *Hyperion*

The Hyperion instrument was designed as a technology demonstration and provides high-quality calibrated data for hyperspectral application evaluation (Pearlman *et al.* 2003a). Hyperion is a high-resolution hyperspectral imager capable of resolving 220 spectral bands (from 0.4 to 2.5 μm) with a 30 m spatial resolution and a nominal spectral resolution of 10 nm. The instrument, which operates on the pushbroom principle, can represent one 7.5 km × 100 km land area per image and can provide detailed spectral mapping across all 220 bands with high radiometric accuracy. The Hyperion has a single telescope and two spectrometers, one visible/near-infrared (VNIR) spectrometer and one short-wave infrared (SWIR) spectrometer. The hyperspectral imaging data acquired with Hyperion has wide ranging applications in mining, geology, forestry, agriculture and environmental management. Detailed classification of land assets with Hyperion enables more accurate application of remotely sensed data, for example, better prediction of crop yield and more accurate assessment of environmental quality (http://eol.gsfc.nasa.gov/Technology/Hyperion.html). Due to low ratio of signal to noise at both spectral ends (<430 nm and >2400 nm), heavy water absorption centred around 1400 and 1900 nm and the spectral overlap of the two spectrometers (VNIR and SWIR), we dropped a total of 75 bands from original 242. Thus a total of 167 bands (effective bands) were used in this analysis. Their wavelength positions and re-ordered band numbers are listed in table 1.

2.2 *ALI*

The ALI employs novel wide field-of-view silicon carbide optics and is a highly integrated multispectral and panchromatic spectrometer. The ALI is a 10-band multispectral system with multiple linear arrays embedded in a single sensor chip assembly (SCA) (Pearlman *et al.* 2003b). Operating in a pushbroom fashion, the ALI provides Landsat type panchromatic and multispectral bands but no thermal band. These bands have been designed to mimic six Landsat bands with three additional bands covering 433–453 nm, 845–895 nm and 1200–1300 nm (table 1).

Table 1. Band numbers and wavelengths of the three sensors: Hyperion, ALI and ETM+ (only those used in this analysis are listed).

Hyperion		ALI		ETM+	
Band	Wavelength (nm)	Band	Wavelength (nm)	Band	Wavelength (nm)
1–90	430–1341	1	433–453	1	450–520
91–124	1462–1795	2	450–515	2	530–610
125–167	1976–2400	3	525–605	3	630–690
		4	630–690	4	780–900
		5	775–805	5	1550–1750
		6	845–895	7	2090–2350
		7	1200–1300		
		8	1550–1750		
		9	2080–2350		

Note: band numbers of Hyperion have been re-ordered. Its nominal band width is 10 nm.

The ALI also contains wide-angle optics designed to provide a continuous $15^\circ \times 1.625^\circ$ field of view (FOV) for a fully populated focal plane, with 30 m resolution for the multispectral pixels and 10 m resolution for the panchromatic pixels. The instrument can represent one 37 km × 100 km land area per image. In this study, we used nine multispectral bands for comparison with the other two sensors.

2.3 *ETM+*

Launched on the Landsat 7 satellite on 15 April 1999, operating by a whiskbroom scanning multichannel radiometer, the ETM+ has six multispectral VNIR and SWIR bands, one panchromatic band and one thermal band with spatial resolutions of 30 m for six VNIR/SWIR bands, 60 m for one thermal band and 15 m for one panchromatic band. The ETM+ replicates the capabilities of the highly successful TM instruments on Landsats 4 and 5. The ETM+ also includes new features that make it a more versatile and efficient instrument for global change studies, land cover monitoring and assessment and large area mapping than its predecessors. The instrument can represent one 185 km × 185 km land area per image. In this study, we used six of these multispectral bands (table 1) for comparison with other two sensors.

3. Study site and datasets

3.1 *Study site*

The study site is at the Blodgett Forest Research Station (120°39′00″ W, 38°54′29″ N) of the University of California, Berkeley, located in the American River watershed on the western slope of the central Sierra Nevada mountain range, El Dorado County, California (figure 1). The Blodgett study area is bounded by a white line in the figure. The vegetation consists of the normal associates of Sierra mixed conifer forest. The major tree species include: five conifers, Sugar pine (*Pinus lambertiana*), Ponderosa pine (*Pinus ponderosa*), White fir (*Abies concolor*), Douglas fir (*Pseudotsuga menziesii*) and Incense cedar (*Calocedrus decurrens*), and one hardwood, California black oak (*Quercus kelloggii*). A species native to the Sierra Nevada but not found in the Blodgett Forest, Giant sequoia (*Sequoiadendron giganteum*), has been planted at the Blodgett research station since the 1900s. In this

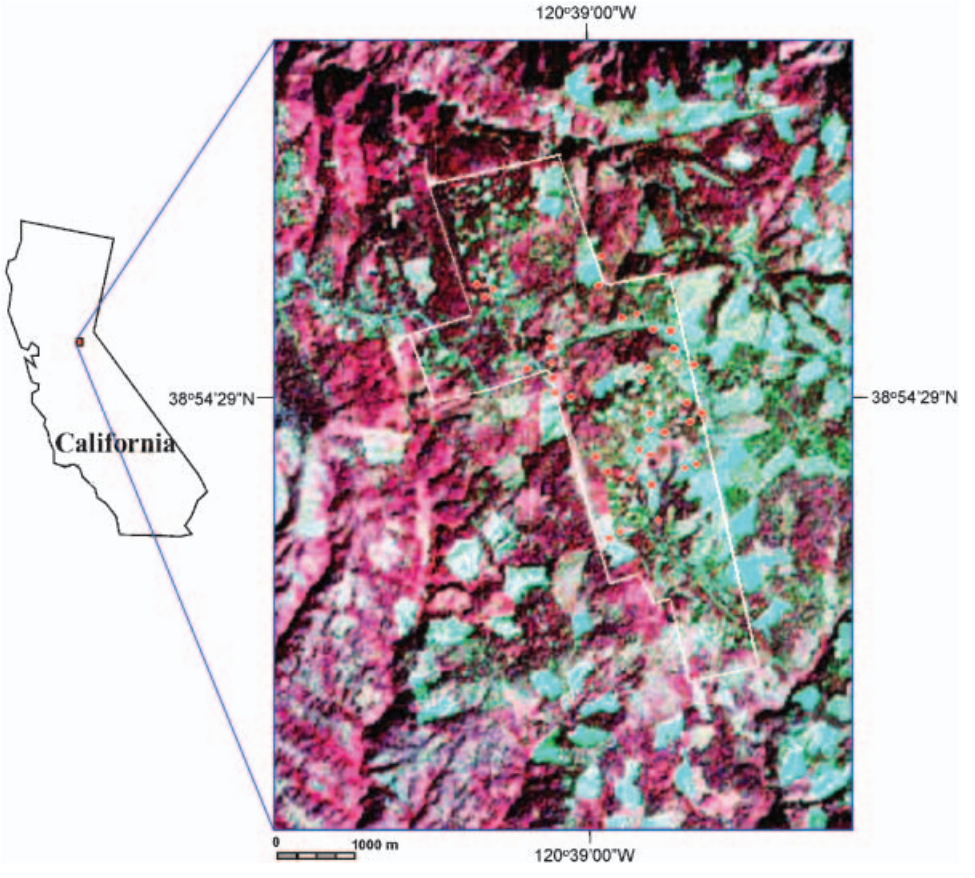

Figure 1. The location of the study site. The positions of plots where forest CC and LAI were collected are marked on the pseudo colour composite image of Hyperion (wavelengths 813/681/548 nm vs R/G/B) by red filled circles.

study, we measured forest CC and LAI both from mixed coniferous forests with the six conifer species in most compartments at the study site.

3.2 *Field CC and LAI measurement*

The forest CC and LAI measurements were carried out on 10–11 August 2001, two months before the acquisition of the three sensors' data. A total of 38 CC and LAI measurements were made in plots typically located within the mixed coniferous forests at the study area. The locations of plots were marked on the pseudo colour composite image of Hyperion (wavelengths 813/681/548 nm vs R/G/B, figure 1) as red filled circles. Each plot is around 2500–3500 m^2 to ensure that 2–4 pixels (30 m resolution) are included from each of the three sensors. We determined a CC measurement from a plot by synthetically considering the results derived from the following procedure. In each field plot, two cross lines were laid out with a 50 m tape. These lines were aligned along approximately S–N and W–E directions across the plot centre. We then measured and summed the intercepted lengths vertically projected by crowns in the overstorey. Finally a CC value (%) was calculated through the formula: CC(%)=sum of intercepted crown lengths/total line length. To

ensure the ability of the CC value to fully represent the plot without bias, we also visually estimated the CC value while measuring it in the plot and interpreted and estimated another CC value from stereo aerial photos. If there exists a significant difference between measured and estimated CC values, we would re-measure the CC measurement from the plot. The natural-colour aerial photos were taken in June 2000 at a scale of approximately 1 : 8000. We used the visually estimated and interpreted CC values to confirm the CC value actually measured in the field.

While measuring the CC value at each plot, we also took an LAI measurement using an LAI-2000 Plant Canopy Analyzer (PCA). The LAI measurement taken by the PCA is the 'effective' LAI (Chen and Cihlar 1996, White *et al*. 1997). Each LAI measurement represents an average of 10 PCA readings that were taken mainly from the overstorey, but including understorey readings of all trees higher than 1.0 m. The locations of PCA readings in each plot were selected based on the canopy closure, age of stands and nutrient level so as to make the measurements representative of the variability within the plot. For plots with an LAI>2.0, almost no understorey was found. Plots whose LAI was lower than 2.0 had a varying proportion of understorey that may have contributed towards LAI measurement. These understoreys consist mostly of broad-leaf species. Because an image pixel spectrum always responds to both the understorey and overstorey, especially in sparse forests, we did not attempt to separate contributions of the understorey and overstorey to the LAI measurement in this study. Since the effective LAI is less variable and easier to measure than LAI, is an intrinsic attribute of plant canopies (Chen and Cihlar 1996), and has also a proportional relationship with LAI (Gower and Norman 1991), we directly use the effective LAI throughout this research and refer to it as LAI.

3.3 *Spectroradiometric measurements*

Between 11:30 and 14:30 on 18 August 2002, we took reflectance measurements in the field from targets of road surface (asphalt and gravel materials), bare soil and young tree canopy (Douglas fir, Giant sequoia, Incense cedar, Ponderosa pine, Sugar pine and White fir) using a FieldSpec®Pro FR (Analytical Spectral Devices, Inc., Boulder, CO, USA). The spectral range covered by the instrument is 350–2500 nm with three separate spectrometers. The first spectrometer has a spectral resolution of 3 nm and the second and third each has a spectral resolution of approximately 10 nm. All spectra were measured at the nadir direction of the radiometer with a 25° FOV. Depending on the target size, the distance between the spectroradiometer and its target was 20 cm to 1 m to allow within-target-area radiance measurement. White reference current was measured every 5–10 min. Each sample was measured 10 times. To ensure that the measurements represented the target, each time we moved the fibre head slightly but ensured that the measurements were from the within-target area. These spectral reflectance measurements were used for atmospheric correction to the ALI and ETM+ data below.

3.4 *Data acquisition from the three sensors*

ALI and Hyperion data for the study site were acquired on 9 October 2001, around 10:30 a.m. local time. Since ETM+ data were not available on the same day as EO-1 data, we used the ETM+ data acquired on 25 October 2001, around 10:30 a.m. local time in this comparative analysis of sensors' data.

4. Analysis methods

4.1 *Retrieving surface reflectance*

Atmospheric correction of hyperspectral data is mandatory for conversion of radiance to reflectance (Goetz *et al*. 2002). Therefore, in this study, atmospheric correction was first conducted to retrieve surface reflectance from data of both the hyperspectral sensor Hyperion and multispectral sensors ALI and ETM+ (in scaled radiance format) using High Accuracy Atmospheric Correction for Hyperspectral Data (HATCH, cf. Qu *et al*. 2003, Goetz *et al*. 2002) and a Simple Atmospheric Correction method (SAC, cf. Gong *et al*. 2003, Pu *et al*. 2003). With the HATCH, atmospheric correction for hyperspectral data of Hyperion was accomplished at the Center for the Study of Earth from Space, Department of Geological Sciences, University of Colorado, USA. HATCH, using its own radiative transfer model rather than the general purpose atmospheric transmission code MODTRAN, improves performance over ATREM (Gao *et al*. 1993) due to implementation of state-of-the-art techniques in the area of atmospheric radiative transfer. The HATCH aims at retrieving surface reflectance spectra of high quality with a reasonable speed. For the ALI and ETM+ data, surface reflectance was retrieved using the SAC method we previously developed. In retrieving surface reflectance with SAC, we first needed three at-sensor total radiances simulated with MODTRAN4 (Berk *et al*. 2000). Thereafter, spectral measurements were taken from targets in the study area and were used to modify the preliminary retrieved surface reflectance. For a detailed SAC procedure, see Gong *et al*. (2003) and Pu *et al*. (2003). All surface reflectance data retrieved from the three sensors are used in following comparative analysis.

4.2 *Comparison methods*

To compare capabilities of the three sensors' data for estimating forest CC and LAI, we designed five comparison methods using univariate and multivariate correlation analysis.

4.2.1 Based on individual bands. Through correlation analysis of all individual bands of the three sensors (167 for Hyperion, nine for ALI and six for ETM+) with 38 forest CC and LAI measurements, we can find which sensor is the most capable of estimating CC and LAI and which bands are the most useful for this estimation. With this method, we can fully compare the three sensors band by band.

4.2.2 Based on ALI band wavelength. The comparison based on the ALI band wavelength relates only to Hyperion and ALI data. We first grouped Hyperion bands located within each single ALI band wavelength, then conducted a correlation analysis of single bands (ALI) and multiple bands (Hyperion) with measured forest CC and LAI. It is evident that one ALI band is properly compared against multiple Hyperion bands. This method emphasizes a comparison between Hyperion and ALI within the single ALI band wavelength rather than considering the number of bands each possesses within the band wavelength.

4.2.3 Based on ETM+ band wavelength. The comparison based on the ETM+ band wavelength can cover all the three sensors because within one ETM+ band wavelength there may be one or multiple ALI or multiple Hyperion bands. Using

the same procedure as in section 4.2.2, we first grouped ALI or Hyperion bands located within each single ETM+ band wavelength, then conducted a correlation analysis of single bands (ETM+) and one or multiple bands (ALI and Hyperion) with measured forest CC and LAI. This method emphasizes a comparison among Hyperion, ALI and ETM+ within the single ETM+ band wavelength rather than considering the differing numbers of bands of the three sensors within the band wavelength.

4.2.4 Based on spectral regions. This comparison method was conducted for all three sensors. To realize this method, the full spectral range (~0.4–2.5 μm) is first divided into three regions: visible (VIS, 0.44–0.73 μm), near-infrared (NIR, 0.73–1.00 μm) and short wave infrared (SWIR, 1.00–2.40 μm). All individual bands of the three sensors are then grouped into corresponding spectral regions based on their individual band wavelengths. To emphasize comparison of ETM+ bands available in the spectral regions, we also grouped ALI and Hyperion individual bands into spectral regions in which just ETM+ bands cover wavelength ranges. Finally, a correlation analysis of the band groups of the three sensors was conducted with measured forest CC and LAI. This method emphasizes a comparison among the three sensors in the same spectral regions rather than considering the differing numbers of their bands within each spectral region.

4.2.5 Based on features or band subset. This method compares the three sensors when they have the same number of features or bands. To utilize the maximum number of ETM+ bands, we set this number at six features or bands for a correlation analysis with measured CC and LAI among all the three sensors. The six bands were selected from 167 Hyperion bands and from nine ALI bands based on a piecewise procedure (SAS 1991) with a criterion of maximum multiple coefficient of correlation (R^2). The six principal components (PCs) were selected from the first 37 PCs (all non-zero PCs) or from the first 20 PCs transformed from 167 Hyperion original bands. The six PCs for ALI were simply selected from the total of nine ALI PCs. The six PCs for Hyperion and ALI were also selected with a criterion of maximum R^2.

4.3 *Statistical test and criterion for correlation analysis*

In this study, two indices were calculated in every comparison analysis that evaluated the capabilities of the three sensors. These indices are univariate/multivariate correlation coefficient (R^2) and the root mean square error (RMSE) predicted by univariate/multivariate regression models. To determine whether the R^2 has statistical significance, a statistic moment μ was calculated with formula (1):

$$\mu = \frac{R^2/m}{(1-R^2)/(n-m-1)} \sim F_\alpha(m, n-m-1) \tag{1}$$

where n and m, respectively, are numbers of samples and variables included in a regression model; F_α can be obtained from an F-distribution table with free degree $1=m$ and free degree $2=n–m–1$. By comparing μ with F_α, the statistically significant degree of a R^2 value can be determined at a certain confidence level. When conducting a multivariate correlation analysis, we adopted a criterion of minimum RMSE to determine the number of variables included in an optimal regression

model. The RMSE was calculated with formula (2):

$$\mathrm{RMSE} = \sqrt{\frac{1}{n-m-1}\sum_{i=1}^{n}\left(y_i - \hat{y}_i\right)^2} \tag{2}$$

where y_i and $\hat{y}_i$ are actual value and predicted value, respectively.

5. Results and analysis

5.1 *Univariatelmultivariate correlation analysis*

One to four homogeneous pixel spectra, corresponding to each of the CC and LAI measurement plots, were extracted from the three calibrated sensors' images. The extracted reflectance spectra were averaged at each measurement plot for correlation calculation of a single or multiple variables with CC and LAI measurements. Using the five comparison methods described above, we calculated correlation coefficients (R^2) and predicted RMSE values of single or multiple variables from the three sensors' data with 38 CC and LAI measurements. The correlation and prediction results with forest CC and LAI are shown in figure 2 for individual band correlation analysis of all the three sensors. Table 2 shows results for Hyperion and ALI sensors based on ALI single band wavelengths, and table 3 for all the three sensors based on ETM+ individual band wavelengths. Table 4 shows results for all the three sensors based on three spectral regions and the available ETM+ band setting, and table 5, again for all the three sensors but based on six features or bands. From the figure and tables, single variable or multi-variable correlation R^2 and regression predicted RMSE using CC are mostly consistent with those using LAI except in table 2 for ALI, table 3 for both ALI and ETM+ and table 4 for ETM+. This is reasonable, considering the fact that there is a correlation between CC and LAI (R^2=0.50, n=38). However, among the three sensors, the best R^2 and RMSE values that are similar when using either CC or LAI vary considerably depending upon band wavelengths or spectral regions or selected features and band groups.

5.2 *Performance of the three sensors*

5.2.1 Based on individual bands. Correlation analysis results of individual bands of the three sensors with forest CC and LAI (n=38) measurements are presented in figure 2(*a–c*). From the figure, it is evident that, for all three sensors, all CC correlation coefficients (R) are higher than the LAI correlation coefficients, except for ETM+ band 4 where the R with CC is a little bit lower than R of LAI. The above results are very reasonable, considering that remote sensing of CC is more direct than of LAI because the CC reflects actual distribution of a given green biomass over a unit area (e.g. a pixel) while LAI generally reaches spectral saturation after LAI=6 or 7 (Peterson and Running 1989). These results agree with the point of view of Chen *et al*. (1999), that if good site averages of CC are obtained, the CC–SR (SR, simple ratio=NIR band/red band) relationship will be better than the LAI–SR relationship because the vertical view is more affected by CC than by LAI. It is also reasonable that CC and LAI are negatively correlated with VIS and SWIR regions of the three sensors, so that the higher the CC and LAI, the less spectral energy is detected by the sensors in the VIS and SWIR regions. This is because the higher the CC and LAI are, the stronger the pigments in the VIS region and the water content and other biochemical components in the SWIR region will absorb spectral energy

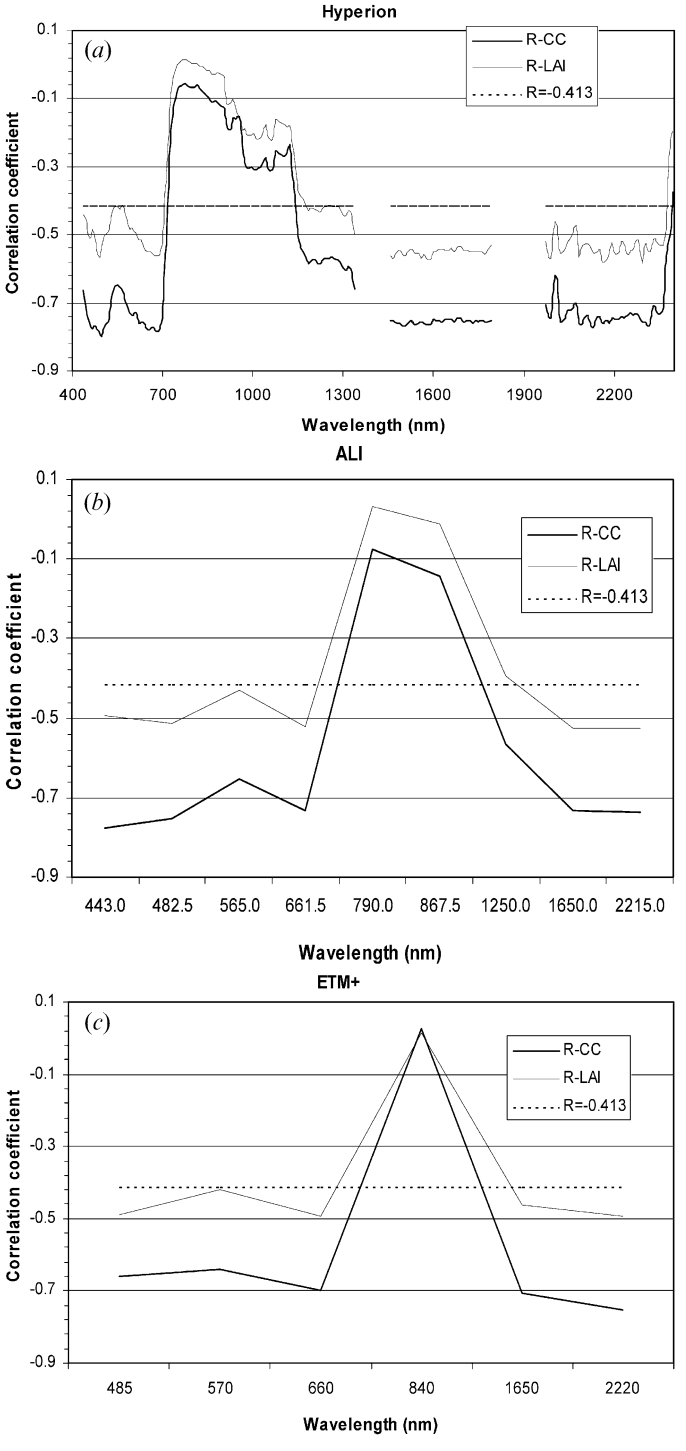

Figure 2. Correlation of individual bands of the three sensors' data: (*a*) Hyperion, (*b*) ALI and (*c*) ETM+, with forest CC and LAI measurements (n=38). The dashed line denotes a correlation coefficient of −0.413 that is statistically significant at a 0.99 confidence level.

Table 2. Comparison of R^2 and RMSE, calculated using data from two sensors, Hyperion and ALI, based on ALI individual band wavelengths with CC and LAI, $n=38$.

ALI			Hyperion		
Band	CC-R^2/RMSE	LAI-R^2/RMSE	Band	CC-R^2/RMSE/n.b.s.	LAI-R^2/RMSE/n.b.s.
1	**0.6052**/13.17**	0.2426**/0.731	1–3	0.5787**/13.61/1	0.2603**/0.723/1
2	0.5650**/13.83	0.2635**/0.721	3–9	0.6490**/12.60/2	0.4014**/0.669/3
3	0.4250**/15.90	0.1832**/0.760	10–18	0.6806**/12.19/3	0.5114**/0.614/4
4	0.5385**/14.24	0.2734**/0.716	20–26	0.6563**/12.47/2	0.4458**/0.644/3
5	0.0057/20.91	0.0010/0.840	34–37	0.1352/19.77/2	0.1348/0.793/2
6	0.0209/20.74	0.0001/0.840	41–46	0.3074**/17.95/3	0.0687/0.822/2
7	0.3201**/17.29	0.1555*/0.772	76–86	0.4800**/15.79/4	0.2505**/0.738/2
8	0.5386**/14.24	**0.2779**/0.714**	100–121	0.7094**/12.59/8	0.6933**/0.528/9
9	0.5453**/14.14	0.2747**/0.716	136–163	**0.8055**/11.10/12**	**0.7080**/0.545/12**

n.b.s. is the number of bands selected. Bold represents the best results in the column.
* and ** denote correlations that are statistically significant at 95% and 99% confidence levels, respectively.

(Curran 1989, Elvidge 1990) (i.e. there is a lower reflectance in these regions). For the three sensors, the R values of all individual bands in both VIS and SWIR regions pass the statistical significance test of linear correlation ($R=-0.413$, dashed line in the figure) at a 0.99 confidence level. However, for the bands in the NIR region, the correlation levels are all very low for all three sensors. The close spectral reflectance between background components (soil, shrub and grasses) and canopy reflectance may be responsible for this low correlation. Among the three sensors, when examining correlation levels with both CC and LAI, we find that many bands of Hyperion in VIS and SWIR consistently have the highest correlation levels compared with ALI and ETM+, except for ALI band 1. This is because the hyperspectral sensor can record subtle spectral information that allows it to be more precise with respect to forest CC and LAI. Comparing the two multispectral sensors, we find that ALI apparently is better than ETM+, especially for bands in the VIS region.

5.2.2 Based on ALI band wavelengths. Table 2 lists correlation analysis results of CC and LAI with two of the sensors: Hyperion and ALI, based on ALI individual band wavelengths. In the table, the number of bands selected for Hyperion data was determined by the minimum RMSE criterion. Generally, the correlation levels for Hyperion data were considerably higher than for ALI data due to the subtle spectral information caught by Hyperion. This did not hold for bands 1–3, corresponding to ALI band 1 wavelength. Specifically, the Hyperion band group corresponding to ALI band 9 wavelength produced the highest correlation with both CC and LAI. This is mainly a function of water content in leaves around 1.9 μm and less atmospheric effect on the Hyperion data than the ALI (Gong *et al.* 2003). For ALI correlation with LAI, the highest R^2 from band 8 also relates to water content in leaves. However for ALI correlation with CC, the highest R^2 is from band 1, which may be due to absorption of pigments greater than that of water and other biochemicals in SWIR region. Since the atmosphere impacts hyperspectral data more seriously than multispectral data, especially on bands in the VIS region for satellite hyperspectral image (Gong *et al.* 2003), a narrow blue band of Hyperion

Table 3. Comparison of R^2 and RMSE, calculated using three sensors' data: Hyperion, ALI and ETM+, based on ETM+ individual band wavelengths with CC and LAI, n=38.

ETM+			ALI			Hyperion		
Band	CC-R^2/RMSE	LAI-R^2/RMSE	Band	CC-R^2/RMSE	LAI-R^2/RMSE	Band	CC-R^2/RMSE/ n.b.s.	LAI-R^2/RMSE/ n.b.s.
1	0.4348**/15.76	0.2376**/0.734	1, 2	**0.6064**/13.34**	0.2650**/0.731	2–9	0.6561**/12.47/2	0.4406**/0.667/5
2	0.4115**/16.08	0.1768**/0.763	3	0.4250**/15.90	0.1832**/0.760	10–18	0.6806**/12.19/3	0.5114**/0.614/4
3	0.4865**/15.02	**0.2429**/0.731**	4	0.5385**/14.24	0.2734**/0.716	20–26	0.6563**/12.47/2	0.4458**/0.644/3
4	0.0008/20.96	0.0003/0.840	5, 6	0.2345**/18.60	0.0849/0.815	34–47	0.6462**/14.67/11	0.2465*/0.751/3
5	0.4991**/14.84	0.2151**/0.745	7, 8	0.5624**/14.07	**0.2962**/0.715**	100–121	0.7094**/12.59/8	0.6933**/0.528/9
7	**0.5640**/13.84**	0.2425**/0.731	9	0.5453**/14.14	0.2747**/0.716	136–163	**0.8055**/11.10/12**	**0.7080**/0.545/12**

n.b.s. is the number of bands selected. Bold represents the best results in the column.
* and ** denote correlation statistically significant at 95% and 99% confidence levels, respectively.

Table 4. Comparison of R^2 and RMSE calculated using data from three sensors, Hyperion, ALI and ETM+, based on three spectral regions: visible (VIS), near-infrared (NIR) and short wave infrared (SWIR) with CC and LAI, $n=38$.

Sensor		VIS (0.44–0.73 μm)	NIR (0.73–1.00 μm)	SWIR (1.00–2.40 μm)
ETM+	Bands	1–3	4	5, 7
	CC-R^2/RMSE	0.4962**/15.31	0.0008/20.96	**0.5726**/13.90**
	LAI-R^2/RMSE	**0.2961**/0.726**	0.0003/0.840	0.2460**/0.740
ALI	ETM+ covers bands	1–4	5, 6	8, 9
	CC-R^2/RMSE	**0.6861**/12.27**	0.2348**/18.60	0.5484**/14.29
	LAI-R^2/RMSE	**0.3514**/0.707**	0.0849/0.815	0.2795**/0.723
	Region covers bands	1–4	5, 6	7–9
	CC-R^2/RMSE	**0.6861**/12.27**	0.2348**/18.60	0.5624**/14.07
	LAI-R^2/RMSE	**0.3514**/0.707**	0.0849/0.815	0.2991**/0.724
Hyper-ion	ETM+ covering bands	2–9, 10–18, 20–16	34–47	100–121, 136–163
	CC-R^2/RMSE/n.b.s.	0.8307**/9.78/9	0.6000*/14.65/9	**0.998**/0.66/30**
	LAI-R^2/RMSE/n.b.s.	0.6543**/0.560/9	0.2465**/0.737/3	**0.9995**/0.042/30**
	Region cover bands	1–30	31–57	58–167
	CC-R^2/RMSE/n.b.s.	0.8944**/8.72/15	0.8887**/10.84/22	**1.0000**/0.10/30**
	LAI-R^2/RMSE/n.b.s.	0.8014**/0.490/16	0.6792**/0.623/16	**1.0000**/0.009/30**

n.b.s. is number of bands selected. Bold represents the best results in the column.
* and ** denote correlations statistically significant at 95% and 99% confidence levels, respectively.

inversely produces a lower correlation compared with ALI band 1. This further proves that the hyperspectral data in the VIS region is sensitive to atmospheric effects, whereas in the SWIR region, the satellite hyperspectral data are less impacted by the atmosphere.

5.2.3 Based on ETM+ band wavelengths. Table 3 lists correlation analysis results (R^2 and RMSE) with CC and LAI for all the three sensors based on six ETM+ individual band wavelengths. In the table, the number of bands selected for Hyperion data was also determined by the minimum RMSE. For comparison between ALI and Hyperion, their correlation levels are similar to those in table 2. Compared to the correlations of ETM+ sensor's data with forest CC and LAI, EO-1 sensors have generated higher correlation with the forest CC and LAI. For ETM+ correlation with CC and LAI, the highest R^2 values come from band 7, as do those for Hyperion data, though ETM+ band 3 has a slightly higher R^2 than band 7 with LAI. Therefore, in general, when examining ETM+ individual band wavelengths, the correlation levels for Hyperion data are the highest among the three sensors while correlation levels for ALI data are higher than those for ETM+ data. Discussions of the results in table 2 in the last paragraph may also apply to those in table 3.

5.2.4 Based on spectral regions. In table 4, all individual bands for the three sensors grouped in the three spectral regions were set up in two scenarios. In the first scenario, all bands located in the three regions for all the three sensors were grouped into three band groups. In the second scenario, all bands located not only in the

Table 5. Comparison of R^2 and RMSE, calculated using six bands or six principal components selected from Hyperion, ALI and ETM+ retrieved reflectance data with CC and LAI, $n=38$.

		CC		LAI	
Sensor	Six variables selected from	R^2/RMSE	Wavelength (nm) or PCs	R^2/RMSE	Wavelength (nm) or PCs
Hyperion	167 bands	**0.8198**/9.59**	497, 589, 609, 681, 2002, 2385	**0.6897**/0.504**	1588, 1992, 2103, 2285, 2295, 2385
	first 37 PCs	0.7746**/10.72	1, 2, 5, 13, 22, 28	0.6029**/0.558	1, 2, 5, 31, 33, 37
	first 20 PCs	0.7673**/10.90	1, 2, 5, 9, 12, 13	0.5232**/0.625	1, 2, 5, 9, 12, 16
ALI	nine bands	0.7349**/11.63	443, 565, 790, 868, 1250, 2215	0.4586**/0.666	483, 565, 662, 790, 1250, 2215
	nine PCs	0.7423**/11.47	1, 2, 4, 5, 6, 8	0.4441**/0.675	1, 2, 3, 5, 6, 7
ETM+	six bands	0.5891/14.48	485, 570, 660, 840, 1650, 2220	0.3068/0.754	485, 570, 660, 840, 1650, 2220

* and ** denote correlations statistically significant at 95% and 99% confidence levels, respectively.
Bold represents the best results in the column.

three regions but also in three ETM+ band groups for Hyperion and ALI data were grouped into another three band groups. In general, for both scenarios, the correlation levels for Hyperion data were the highest among the three sensors while correlation levels for ALI data were better than those for ETM+ data. For the three ALI band groups, the highest correlations with both CC and LAI were from VIS region. This implies that ALI band 1 (433–453 nm) with a band width of 20 nm is a good prospect for future Landsat data continuity. Due to a higher number of bands in the band groups for Hyperion data, correlations produced by every band group with CC and LAI are significant at a 95% confidence level. Again, higher correlation results appeared in the SWIR region for Hyperion data because, consistent with our previous work (Gong *et al*. 2003), the Hyperion data are less influenced by the atmosphere and have a direct correlation association with spectral absorption of water in tree leaves.

5.2.5 Based on features and band subset. In early correlation analysis (tables 2–4) with forest CC and LAI, we emphasized the same band wavelengths or same spectral regions rather than considering differing numbers of bands among the three sensors. In this comparison, we emphasized use of the same number (fixed 6) of features (principal components, PCs) or bands selected by the piecewise procedure with an optimal R^2. Table 5 lists correlation analysis results (R^2 and RMSE) with both CC and LAI from 6 PCs or six band subsets. For Hyperion data, six bands were selected from all 167 reflectance bands and two six-PCs were selected from a total of 37 non-zero PCs (i.e. accounting for 100% of total variance included in the database) and from the first 20 PCs (accounting for 99.67% of total variance included in the database), respectively. For ALI data, six bands and six PCs were selected from all nine original bands and all nine PCs, respectively, while for ETM+ data, all six original bands were used. Generally, from the table, it is obvious that either the six-band subset or the six PCs correlated with CC and LAI for Hyperion, their R^2 and RMSE are all consistently better than those of other two sensors. The results from ALI are better than those from ETM+. The experimental results agree with those analysed above. Specifically, for Hyperion, the six bands selected for correlation with CC include four bands in VIS region and two bands in SWIR while all six bands selected for LAI are in SWIR only. There are two reasons for this. First, for LAI, since LAI has a close relation with green biomass, whose spectral characteristics are mainly accounted for by water contained in green leaves (Elvidge 1990), all six bands selected from the SWIR region should be reasonable. Second, for CC, because the CC reflects the total absorption of spectral energy either through a distribution of a given green biomass over a unit area as addressed early or by water absorbing spectral energy in the SWIR region and pigments (mainly chlorophyll contents) in the VIS region, the four visible bands included in the six-band subset seemed reasonable too. For the six PCs of Hyperion, the first three PCs included are the same (PCs 1, 2 and 5) between CC and LAI correlation analysis. This indicates that the first two PCs accounting for 95.03% of total variance are a major part of the six PCs correlation analysis and that the remaining four PCs function in a supplementary way. For ALI, the six bands and six PCs selected were similar for correlation between CC and LAI. Both groups of six bands come from all three spectral regions. This may be caused by broader and fewer bands compared with Hyperion. The R^2 and RMSE for ALI data with CC or LAI are similar between the six-band and six-PC multiple variables.

6. Conclusions

In this study, multispectral and hyperspectral remote sensing data were acquired from the Hyperspectral Imager (Hyperion) and Advanced Land Imager (ALI) onboard the EO-1 satellite on 9 October 2001 and from Landsat ETM+ on 25 October 2001. A total of 38 mixed coniferous forest crown closure (CC) and LAI measurements were collected at Blodgett Forest Station, University of California at Berkeley, USA. The correlation analysis results of the three sensors' data with the forest CC and LAI measurements were used for evaluating capabilities of the three sensors for estimating forest CC and LAI. The experimental results indicate: (1) higher individual band correlations with CC and LAI appear in visible (VIS) and short wave infrared (SWIR) regions due to spectral absorption features (pigments in VIS and water and other biochemicals in SWIR); (2) based on ALI individual band wavelengths, the correlation/RMSE produced with Hyperion bands are all better than those produced with ALI except for ALI band 1 due to atmospheric scattering of Hyperion bands in the VIS region; (3) based on ETM+ individual band wavelengths, Hyperion is better than ALI, which is in turn better than ETM+, especially for the NIR band group of Hyperion; (4) based on spectral regions, again, Hyperion is better than ALI, which is in turn better than ETM+, and optimal results appear in the VIS region for ALI and in the SWIR region for Hyperion; and (5) if just considering six bands or six features (six principal components) for estimating CC and LAI, optimal results are obtained from the six bands selected from a total of 167 Hyperion bands.

Generally speaking, for estimation of forest CC and LAI in this study, the Hyperion sensor has outperformed the ALI and ETM+ sensors, whereas ALI is better than ETM+. Hyperion has produced the best results for estimating forest CC and LAI due to its high spectral resolution that can record subtle spectral information, which is useful for estimating the forest CC and LAI. Another advantage of the Hyperion sensor is that its SWIR data are lightly affected by the atmosphere (mainly absorption), except two major water absorption bands. Therefore, the best spectral region for Hyperion is SWIR, but for ALI and ETM+, the visible region should be considered for use instead. From this experiment comparing the three sensors for estimating forest CC and LAI, the Hyperion sensor has demonstrated its potential for application in forest management and ecosystem studies. Since ALI band 1 (433–453 nm) with a band width of 20 nm is influenced by the atmospheric scattering less than bands of Hyperion, ALI band 1 may be a good prospect for future Landsat data continuity.

Acknowledgements

This research was partially supported by a NASA EO-1 science validation grant (NCC5-492). The authors would like to express thanks to Leo Wang, Yong Tian, Paihui Hsu and Qi Chen for their help in the fieldwork. Atmospheric correction to Hyperion in this study was carried out by the Center for the Study of Earth from Space, Department of Geological Sciences, University of Colorado, USA.

References

Barry, P.S., Mendanhall, J., Jarecke, P., Folkman, M., Pearlman, J. and Markham, B., 2002, EO-1 Hyperion hyperspectral aggregation and comparison with EO-1 Advanced Land Imager and Landsat 7 ETM+. *2002 IEEE International Geoscience*

and Remote Sensing Symposium and the 24th Canadian Symposium on Remote Sensing, *Toronto, Canada, 24–28 June 2002* (Piscataway, NJ: IEEE), III, pp. 1648–1651.

BERK, A., ANDERSON, G.P., ACHARYA, P.K., CHETWYND, J.H., BERNSTEIN, L.S., SHETTLE, E.P., MATTHEW, M.W. and ADLER-GOLDEN, S.M., 2000, *MODTRAN4 User's Manual*, Air Force Research Laboratory, Hanscom AFB, MA, pp. 1–93.

BRYANT, R., MORAN, M.S., MCELROY, S., HOLIFIELD, C., THOME, K. and MIURA, T., 2002, Data continuity of Landsat-4 TM, Landsat-5 TM, Landsat-7 ETM+, and Advanced Land Imager (ALI) sensors. *2002 IEEE International Geoscience and Remote Sensing Symposium and the 24th Canadian Symposium on Remote Sensing*, *Toronto, Canada, 24–28 June 2002* (Piscataway, NJ: IEEE), I, pp. 584–586.

CHEN, J. and CIHLAR, J., 1996, Retrieving leaf area index of boreal conifer forests using Landsat TM images. *Remote Sensing of Environment*, **55**, pp. 153–162.

CHEN, J.M., LEBLANC, S.G., MILLER, J.R., FREEMANTLE, J., LOECHEL, S.E., WALTHALL, C.L., INNANEN, K.A. and WHITE, H.P., 1999, Compact Airborne Spectrographic Imager (CASI) used for mapping biophysical parameters of boreal forests. *Journal of Geophysical Research*, **104**, pp. 27945–27958.

CURRAN, P.J., 1989, Remote sensing of foliar chemistry. *Remote Sensing of Environment*, **30**, pp. 271–278.

ELVIDGE, C.D., 1990, Visible and near infrared reflectance characteristics of dry plant materials. *International Journal of Remote Sensing*, **11**, pp. 1775–1795.

FANG, Y.-C., 1980, Aerial photo and Landsat image use in forest inventory in China. *Photogrammetric Engineering and Remote Sensing*, **46**, pp. 1421–1424.

FASSNACHT, K.S., GOWER, S.T., MACKENZIE, M.D., NORDHEIM, E.V. and LILLESAND, T.M., 1997, Estimating the leaf area index of north central Wisconsin forests using the Landsat thematic mapper. *Remote Sensing of Environment*, **61**, pp. 229–245.

GAO, B.-G., HEIDEBRECHT, K.B. and GOETZ, A.F.H., 1993, Derivation of scaled surface reflectances from AVIRIS data. *Remote Sensing of Environment*, **44**, pp. 165–178.

GERYLO, G.R., HALL, R.J., FRANKLIN, S.E. and SMITH, L., 2002, Empirical relations between Landsat TM spectral response and forest stands near Fort Simpson, Northwest Territories, Canada. *Canadian Journal of Remote Sensing*, **28**, pp. 68–79.

GOBRON, N., PINTY, B. and VERSTRAETE, M.M., 1997, Theoretical limits to the estimation of the leaf area index on the basis of visible and near-infrared remote sensing data. *IEEE Transactions on Geoscience and Remote Sensing*, **35**, pp. 1438–1445.

GOETZ, A.F.H., FERRI, M., KINDEL, B. and QU, Z., 2002, Atmospheric correction of Hyperion data and techniques for dynamic scene correction. *2002 IEEE International Geoscience and Remote Sensing Symposium and the 24th Canadian Symposium on Remote Sensing*. *Toronto, Canada, 24–28 June 2002* (Piscataway, NJ: IEEE), III, pp. 1408–1410.

GONG, P., PU, R. and MILLER, J.R., 1995, Coniferous forest leaf area index estimation along the Oregon transect using compact airborne spectrographic imager data. *Photogrammetric Engineering and Remote Sensing*, **61**, pp. 1107–1117.

GONG, P., PU, R., BIGING, G. and LARRIEU, M.R., 2003, Estimation of forest leaf area index using vegetation indices derived from Hyperion hyperspectral data. *IEEE Transactions on Geoscience and Remote Sensing*, **41**, pp. 1355–1362.

GOODENOUGH, D.G., BHOGAL, A.S., DYK, A., HOLLINGER, A., MAH, Z., NIEMANN, K.O., PEARLMAN, J., CHEN, H., TAN, T., LOVE, J. and MCDONALD, S., 2002, Monitoring forest with Hyperion and ALI. *2002 IEEE International Geoscience and Remote Sensing Symposium and the 24th Canadian Symposium on Remote Sensing*, *Toronto, Canada, 24–28 June 2002* (Piscataway, NJ: IEEE), II, pp. 882–885.

GOWER, S.T. and NORMAN, J.M., 1991, Rapid estimation of leaf area index in conifer and broad-leaf plantations. *Ecology*, **72**, pp. 1896–1900.

GUYOT, G., GUYON, D. and RIOM, J., 1989, Factors affecting the spectral response of forest canopies: a review. *Geocarto International*, **4**, pp. 3–18.

HALL, R.J., FRANKLIN, S.E., GERYLO, G.R. and ROBERTS, A., 1999, Estimation of crown closure and species composition from high resolution multispectral imagery. In *Automated Interpretation of High Spatial Resolution Digital Imagery for Forestry, Victoria, British Columbia, Canada, 10–12 February 1998*, D.A. Hill and D.G. Leckie (Eds) (co-published by Ministry of Forests, B.C., and MacMillan Bloedel Ltd, Canada), pp. 309–320.

HU, B., INANNEN, K. and MILLER, J.R., 2000, Retrieval of leaf area index and canopy closure from CASI data over the BOREAS flux tower sites. *Remote Sensing of Environment*, **74**, pp. 255–274.

PEARLMAN, J.S., BARRY, P.S., SEGAL, C., SHEPANSKI, J., BEISO, D. and CARMAN, S., 2003a, Hyperion, a space-based imaging spectrometer. *IEEE Transactions on Geoscience and Remote Sensing*, **41**, pp. 1160–1173.

PEARLMAN, J.S., CRAWFORD, M., JUPP, D.L.B. and UNGAR, S., 2003b, Foreword to the Earth Observing 1 special issue. *IEEE Transactions on Geoscience and Remote Sensing*, **41**, pp. 1147–1148.

PETERSON, D.L. and RUNNING, S.W., 1989, Chapter 10: Applications in forest science and management. In *Theory and Applications of Optical Remote Sensing*, Wiley Series in Remote Sensing, G. Asrar (Ed) (New York: John Wiley & Sons), pp. 429–473.

PU, R., GONG, P. and BIGING, G., 2003, Simple calibration of AVIRIS data and LAI mapping of forest plantation in southern Argentina. *International Journal of Remote Sensing*, **24**, pp. 4699–4714.

QU, Z., KINDEL, B.C. and GOETZ, A.F.H., 2003, The High Accuracy Atmospheric Correction for Hyperspectral Data (HATCH) model. *IEEE Transactions on Geoscience and Remote Sensing*, **41**, pp. 1223–1231.

SAS INSTITUTE INC., 1991, *SAS/STA User's Guide,* release 6.03 edition (Cary, NC: SAS Institute Inc.).

UNGAR, S., PEARLMAN, J., MENDENHALL, J. and REUTER, D., 2003, Overview of the Earth Observing One (EO-1) mission. *IEEE Transactions on Geoscience and Remote Sensing*, **41**, pp. 1149–1159.

US DEPARTMENT OF AGRICULTURE, 1968, *Timber Management Plan Inventory Handbook,* Forest Service, USDA, 2441.1 R5 Supplement no. 65.

WHITE, J.D., RUNNING, S.W., NEMANI, R., KEANE, R.E. and RYAN, K.C., 1997, Measurement and remote sensing of LAI in Rocky Mountain Montane ecosystems. *Canadian Journal of Forest Research*, **27**, pp. 1714–1727.